Title of Publication *Edited by*
TMS (The Minerals, metals & Materials Society), 2007

SCATTERING ON OVERLAPPING STRAIN FIELDS CAUSED BY DEFECTS GROUPINGS

R.I. Barabash, E.D. Specht, G.E. Ice
Materials Science and Technology Division
Oak Ridge National Laboratory, Oak Ridge TN 37831

Keywords: diffuse scattering, coherent precipitate, strain field

Abstract

The grouping of point defects into clusters, microscopic pores, coherent precipitates, dislocation loops and other organized structures, changes the character of the local strain field and results in a redistribution of diffuse scattering intensity.
The diffuse scattering depends on both the local and the average lattice distortions. The average distortion is described by the static Debye-Waller factor exponent 2W. For point defects typically 2W<<1. Grouping of point defects increases this value and eventually results in conditions where 2W>>1. Diffuse scattering distributions for different ranges of static Debye-Waller factor are considered.

Introduction

A qualitative classification of defects with respect to their influence on reciprocal space has been developed by Krivoglaz [1]. This classification is based on an analysis of the static Debye-Waller Factor (DWF) exponent, e^{-2W}. Defects can be described as belonging to one of two kinds:

<u>Defects of the 1st kind:</u> In crystals with defects of the 1st kind, the intensity from the Bragg peaks is redistributed into broad diffuse intensity. In addition, the Bragg peaks remain sharp like those of perfect crystals, but become weaker and can be displaced from their reciprocal space location without defects. For this reason, both the Bragg and Diffuse scattering can be simultaneously observed in the diffraction pattern. Usually, the intensity of the diffuse component I_D increases and the intensity of the Bragg component I_0 decreases with defect concentration *c*.

<u>Defects of the 2nd type:</u> In crystals with defects of the second kind, long-range spatial correlations of atomic sites are lost and the Bragg term becomes meaningless. Sharp Bragg reflections of perfect crystals are replaced by Broad peaks which can be anisotropic in reciprocal space. Typically broadening increases with defect concentration.

Whether a defect is of the 1st or 2nd kind depends on the behaviour of the DWF at large distances ($\rho \Rightarrow \infty$). It should be noted that DWF has a complicated dependence on the details of the distortion fields near a defect. As a first approximation,

$$2W = \mathrm{Re}\, T_\infty \cong c \lim_{\rho \Rightarrow \infty} \sum_t \left[1 - Cos(\boldsymbol{Q}\boldsymbol{u}_{ss't})\right]\left[1 + \frac{1}{F}\left(\varphi_{st} + \varphi_{s't}\right)\right] \qquad (1)$$

Here T_∞ is the correlation function for defects at large distances ($\rho \Rightarrow \infty$), c is the concentration of defects, F is the structure factor of the average crystal, Q is the momentum transfer for certain (*hkl*) reflection**,** $u_{ss't}$ is the difference between displacements in two scattering cells *s* and *s'* caused by the defect located in the position *t*, and φ_{st} and $\varphi_{s't}$ describe structure amplitude changes of scattering cells *s* and *s'* caused by the defect located in the position *t*. We note that for dislocations, changes in structure amplitudes are small and the behavior of the *2W* depends mainly of the asymptotic behavior of the displacement field created by the dislocation. With defects there are two possibilities: *2W* is either finite at large distances or *2W* tends to infinity at the large distances. It was shown [1, 2] that if the displacements fall off faster then $1/r^{3/2}$, then the value *2W* is finite, and the defects belong to the 1st kind. If the displacements decrease lower then $1/r^{3/2}$, then the value $2W \Rightarrow \infty$, and these defects are of the 2nd kind.

In this study we report the diffuse scattering analysis of coherent precipitates which are defects of the 1st kind (Fig. 1). As described above, these defects cause diffuse scattering, $I_D(\boldsymbol{Q})$, that exists together with regular (strong) Bragg reflections, $I_{Bragg}(\boldsymbol{Q})$ [1, 2].

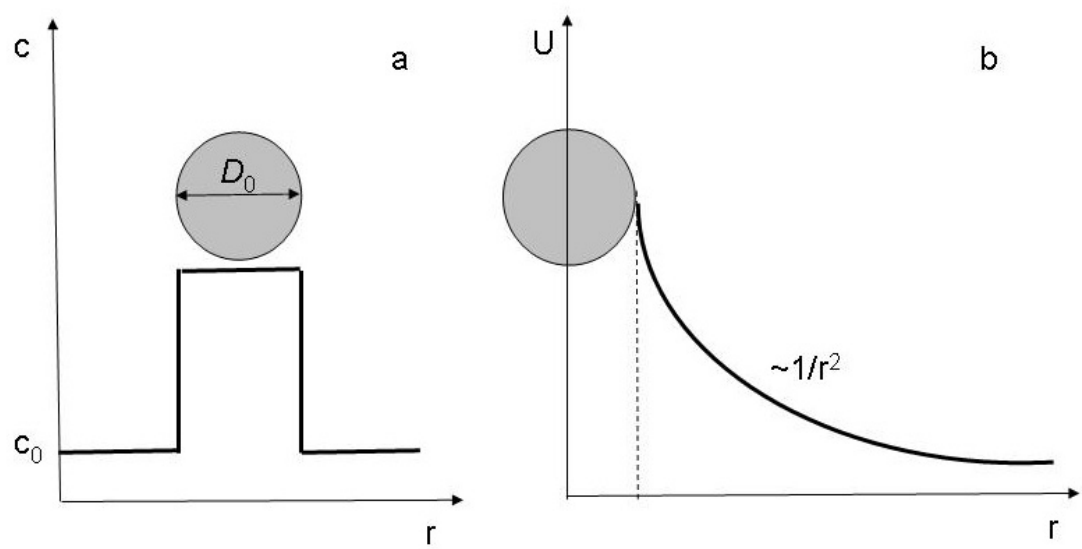

Figure1. Model of the concentration distribution around a precipitate with a sharp boundary (a), and strain filed (b) in the vicinity of the precipitate.

The Bragg positions are displaced relative to the ideal positions of the matrix without precipitates. The analysis of the diffuse scattering differs for the case of small values $2W \leq 1$ (weak distortions) and large values $2W >> 1$ (strongly distorted solids). Many examples of the diffuse scattering analysis for crystals with defects of the 1st kind are described in the literature [1 - 20]. When $2W \leq 1$ it is often possible to use a single defect approximation in the isotropic matrix [4-8]. In many cases when $2W >> 1$ and even $2W \sim 1$ the overlapping strain fields interact and single defect approximation cannot be used any more. We will follow the approach [1, 2] which gives the possibility to handle the overlapped strain fields in the matrix.
The intensity distribution *I (q)* of x-ray (or neutron) scattering due to defects can be computed from the expression:

$$I(\boldsymbol{Q}) = \left| \sum_i f_i \exp(i\boldsymbol{Q} \bullet (\boldsymbol{R}_i^0 + \boldsymbol{u}_i)) \right|^2 \qquad (2)$$

Here f_i is the scattering factor from an individual atom *i*, with relaxed co-ordinates $R_i = \mathbf{R}_i^0 + \mathbf{u}_i$ due to the presence of defects. Here $\mathbf{u}_i$ is the displacement from the equilibrium positions $\mathbf{R}_i^0$ corresponding to the undeformed crystal. We calculate the $\mathbf{u}_i$ using continuum elastic theory. $\boldsymbol{Q} = \boldsymbol{k}_2 - \boldsymbol{k}_1$ is the diffraction vector with $\boldsymbol{k}_1$ and $\boldsymbol{k}_2$ being wave vectors of the incident and scattered x-rays.

Experimental Details

Diffuse scattering measurements were made using bending magnet radiation at beamline 33-BM-C of the Advanced Photon Source. 22 keV x-rays were selected using a sagitally focusing double crystal Si (111) monochromator. A pair of Rh-coated mirrors was used to eliminate harmonics and to focus the beam meridionally. The focal spot was ~0.6 mm in diameter.
Thermal diffuse scatter was suppressed by cooling the samples to ~6 K using a closed-cycle He refrigerator. Compton scattering and x-ray fluorescence were resolved from elastic scattering using an energy-dispersive Vortex™ Si drift detector. Incident x-ray flux was monitored using an air-filled ion chamber. Slits were used to define the instrumental resolution. Resolution varies with scattering angle and slit dimensions; at low angles the resolution was 0.0012 $Å^{-1}$ in the radial and 0.0024 $Å^{-1}$ in the transverse direction; far from the Bragg reflections, the slits were widened to increase signal. Reciprocal space units are $Q = 4\pi \sin\theta / \lambda$ where *Q* is the momentum transfer, θ is the Bragg angle, and λ is the wavelength. Ti filters were used to reduce the beam intensity near Bragg reflections so the detector was not saturated.
The samples were needle shaped (10mm × 0.5mm diameter) ternary Ni-Al-Si alloys with a 11.9 %Al and 2.1%Si corresponding to the boundary region between the γ solid solution and ordered Ni_3Al-based γ' phase with L_12 structure. The sample was quenched and stress annealed. The direction of the stress was along [100] direction and coincided with the needle axes.

Results and Discussion

Shape function of the precipitate

Scattering by inhomogeneous solid solutions with precipitates is described by Eq. (2). We consider the following simple model:
Ordered precipitates with long- range order parameter η and with sharp (but coherent) boundaries formed in the disordered matrix (Fig. 1). We assume an average precipitates size D_0. The shapes of the precipitates are assumed to be the same. We use the shape function which was first introduced by Ewald [1].

Let us describe the shape of the precipitates (P) with shape function $s_p(\mathbf{r}-\mathbf{R}_{mp}) = \begin{cases} 1(inside P) \\ 0(outside P) \end{cases}$ of the precursors (Fig. 1). $\mathbf{R}_{mp}$- characterizes the position of the *m*-th precursor center. Matrix shape function is equal $s_m(\mathbf{r}) = \begin{cases} 1(outside P) \\ 0(inside P) \end{cases}$.
The diffuse scattering intensity in weakly distorted crystals can be then re written:

$$I_D(\boldsymbol{Q}) = \left| f_A - f_B \right|^2 \left\langle \left| a_D(\boldsymbol{Q}) \right|^2 \right\rangle, \qquad a_D(\boldsymbol{Q}) = \sum_{s=1}^{N} f_s \exp(i\boldsymbol{QR}) . \tag{3}$$

Here $a_D(\boldsymbol{Q})$ is the amplitude of scattering. $a_D(\boldsymbol{Q})$ can be calculated by means of approximation the sum by an integral over the whole space:

$$a_D(\boldsymbol{Q}) = f \int Y^{\infty}(\boldsymbol{r}) s(\boldsymbol{r}) \exp(i\boldsymbol{Qr}) d\boldsymbol{r}, \quad \text{with } Y^{\infty}(\mathbf{r}) = \sum_{s=1}^{\infty} \delta(\mathbf{r}-\mathbf{R}_s) . \tag{4}$$

Here the summation over *s* in the last expression for $Y^{\infty}(\mathbf{r})$ is performed over the lattice sites of the *infinite* ideal lattice with δ -functions in each lattice site $\mathbf{R_s}$. This means that $Y^{\infty}(\mathbf{r})$ is a periodic function. In the integral for $a_D(\boldsymbol{Q})$ this function $Y^{\infty}(\mathbf{r})$ is multiplied by shape function ***s(r)*** equal 1 inside the crystal and 0 outside it. This allows integration over the whole sample volume. The amplitude of scattering $a_D(\boldsymbol{Q})$ is written as a Fourier transform of the product $Y^{\infty}(\mathbf{r})$ and ***s(r)***. We take into account that the Fourier integral of the product of two functions is determined as a convolution of Fourier integrals of those two components:

$$a_D(\boldsymbol{Q}) = \frac{f}{(2\pi)^3} \int Y^{\infty}(\boldsymbol{k}) s(\boldsymbol{Q}-\boldsymbol{k}) d\boldsymbol{k} . \tag{5}$$

Here ***s(q)*** is Fourier integral of the shape function:

$$s(\mathbf{q}) = \int s(\mathbf{r}) \exp(i\mathbf{qr}) d\mathbf{r} . \tag{6}$$

integration over ***dk*** as well as over ***dr*** is performed over the whole space.

Scattering by weakly distorted matrix with precipitates

In weakly distorted solids the DWF exponent $2W \sim 1$. Consider a simple model of similar randomly distributed precipitates, with a minimal size of R_0, straining the cubic matrix due to the size misfit. In the immediate vicinity of the reciprocal lattice point when the condition $q << 1/R_0$ is valid, the strain induced distortions in the cubic matrix, follows a $1/r^2$ dependence,

$$\left|\boldsymbol{U}(\boldsymbol{r})\right| \sim C/r^2 \quad . \tag{7}$$

Here C is the force constant of the precipitate and r is the distance from the precipitate. Precipitate induced strain, changes the intensity of scattering. Moreover the structure factor F_p of a precipitate differs from the structure factor of the matrix. If precipitate and matrix have the same structure and are coherent (the difference of structure factor can be defined as $\Delta F = F - F_p$. Strain induced changes of the scattered intensity are typically coupled with the structure factor induced changes. This is the case of FCC Ni-based alloys with L_12 Ni_3Al- based precipitates.
In the vicinity of the matrix reciprocal lattice points the diffuse scattering intensity can be written as:

$$I_D = \frac{N_p e^{-2W}}{v^2}\left|\Delta F - F\boldsymbol{Q}\boldsymbol{A}_{\boldsymbol{q}}\right|^2 \left|s(\boldsymbol{q})\right|^2 . \tag{8}$$

Here v is a unit cell volume; N_p is the number of precipitates in the probed volume, $\boldsymbol{A}_{\boldsymbol{q}}$ depends on the Fourier transform of the precipitate induced strain in the matrix. For cubic precipitates in the cubic matrix

$$\boldsymbol{A}_{\boldsymbol{q}X} = 3L\left(C_{11} + 2C_{12}\right)\left(1 + \xi n_Y\right)\left(1 + \xi n_Z^2\right)/3Dq . \tag{9}$$

Here $L\delta_{ij}$ is a self deformation tensor of the precipitate; D is a function of matrix anisotropy parameter, ξ, elastic moduli tensor components, C_{11}, C_{12}, C_{44} and direction in the reciprocal space $\boldsymbol{n} = \boldsymbol{q}/q$. Other $\boldsymbol{A}_{\boldsymbol{q}}$ components can be similarly written.
In the following discussion, three different cases will be distinguished: (a) strain induced scattering; (b) structure factor induced scattering; (b) coupled strain and structure factor induced scattering.
At larger distances from the ideal reciprocal lattice point $q >> 1/R_0$ and diffuse scattering intensity drops off faster, for instance for spherical precipitates, as $1/q^4$. We

use the change of this q dependence of intensity to estimate the size of the coherent precipitate.

<u>Diffuse scattering by solids with coherent precipitates near the superlattice peak</u>

If precipitates have significantly larger elastic moduli then their matrix (as in the case of ordered L_12 type Ni_3Al based γ' precipitates) then they usually create strong distortion fields in the surrounding matrix, while in the precipitates themselves the strain level is low. In this case and assuming no correlation between the precipitates, the diffuse scattering intensity around the superlattice peaks can be written as

$$I_D(\boldsymbol{Q}) = \frac{\left|F_{Ni_3Al}\right|^2}{v^2} \sum_{G'} \sum_{\alpha=1}^{\lambda} N_{p\alpha} \left|s_\alpha\left(\boldsymbol{Q}-\boldsymbol{G}'\right)\right|^2 , \tag{10}$$

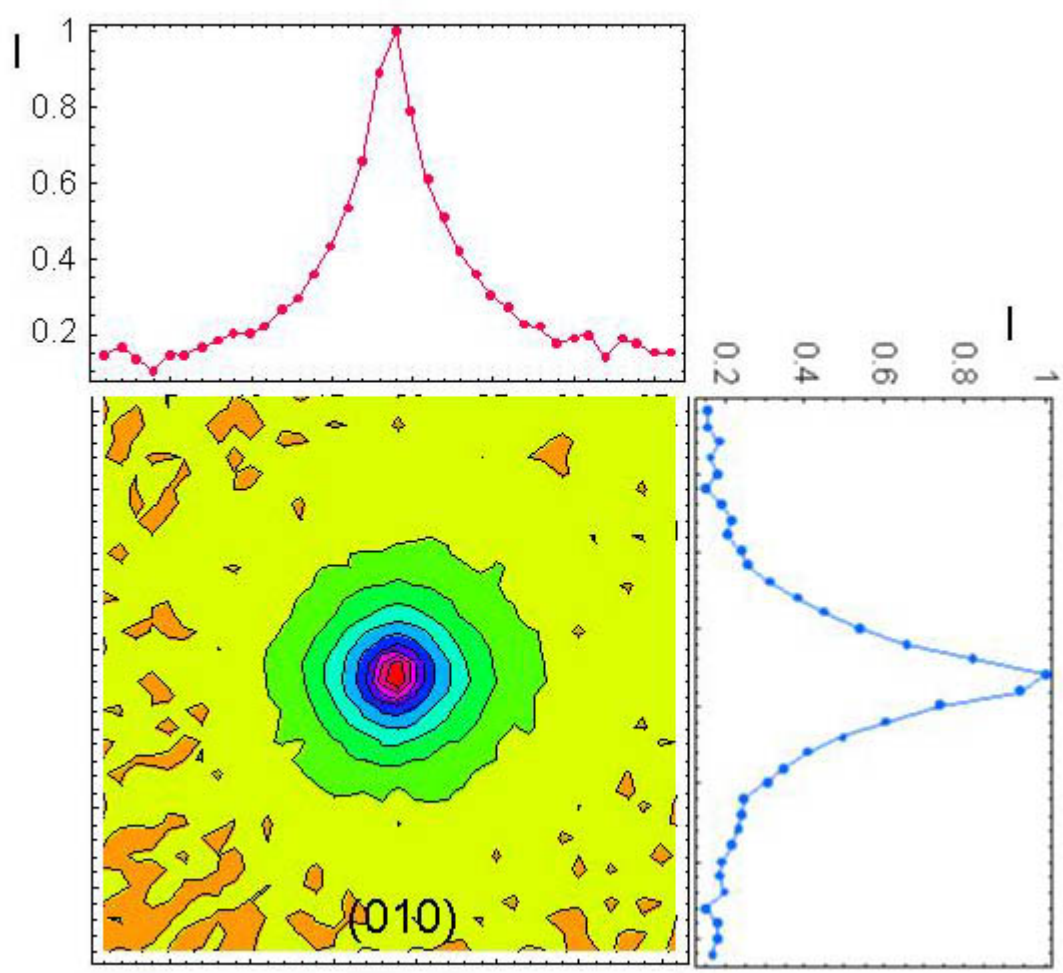

Figure 2. Logarithmic map of intensity around the superlattice (010) reflection. Normalized intensity profiles along and transverse to the diffraction vector are shown on both sides of the map.

where $N_{p\alpha}$ is a number of α type precipitates in the probed volume, F_{Ni_3Al} is a structure factor of the superlattice reflection. In this case, $I_D(\boldsymbol{Q})$ has a maximum at ***Q=G'*** , (***Q*** is the diffraction vector and ***G'*** is a reciprocal lattice vector of the superlattice site) and depends only on the shape function of the precursors of the regions with long range correlation $|s_\alpha(\boldsymbol{q})|^2$. Eq. (10) for $I_D(\boldsymbol{Q})$ describes an intensity distribution around the superlattice peak with FWHM $\approx 2\pi / D_0$.

An experimental diffuse intensity contourmaps around the (010) superlattice reflection together with intensity profiles in q_X and q_Y directions are shown in Fig. 2. Assuming that there is no correlation between precipitates we estimated the precipitates size from the analysis of superlattice reflections with small (100) type Miller indices. Intensity profiles were measured for four orders of similar reflections (100, 300, 500, 700) (<100> type reflections for both [100] and [010] directions and used to determine the size of coherent precipitates in two orthogonal directions. Fig. 3a shows the dependence of the FWHM of the <100> and <010> type superlattice reflections on the order of the reflection. The broadening of the superstructure reflections is insensitive to H and is due to the small size of precipitates. In the analyzed sample the precipitates size was ~92A along and ~77A perpendicular to the stress annealing direction.

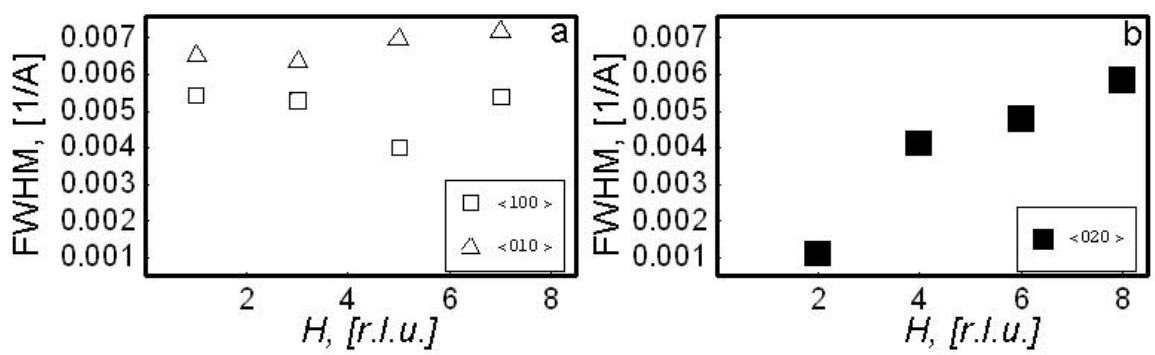

Figure 3. FWHM dependence on H: (a) the <100> type (open squares) and <010> type (open triangles) superstructure reflections; (b) fundamental <020> type reflections (filled squares).

<u>Diffuse scattering near the fundamental reflections</u>

When the matrix is relatively weakly distorted, the DWF related to distortion fields around precipitates is of the order of unity: $Exp(-2W) \sim 1$. The presence of coherent precipitates causes local lattice distortions due to the lattice mismatch between the matrix and the precipitate $|\boldsymbol{u}(\boldsymbol{r})| \sim C / r^2$ (with C being the strength constant of the precipitate). In contrast to the superstructure reflections the FWHM of the fundamental reflections increases with H (Fig. 3b) which is typical for precipitation induced strain broadening. The structure factor F also changes in the region occupied by the precipitate. Distortions

of the lattice together with the changes of the structure factor in the volume occupied by the precipitate cause asymmetry of the diffuse scattering distribution around the regular

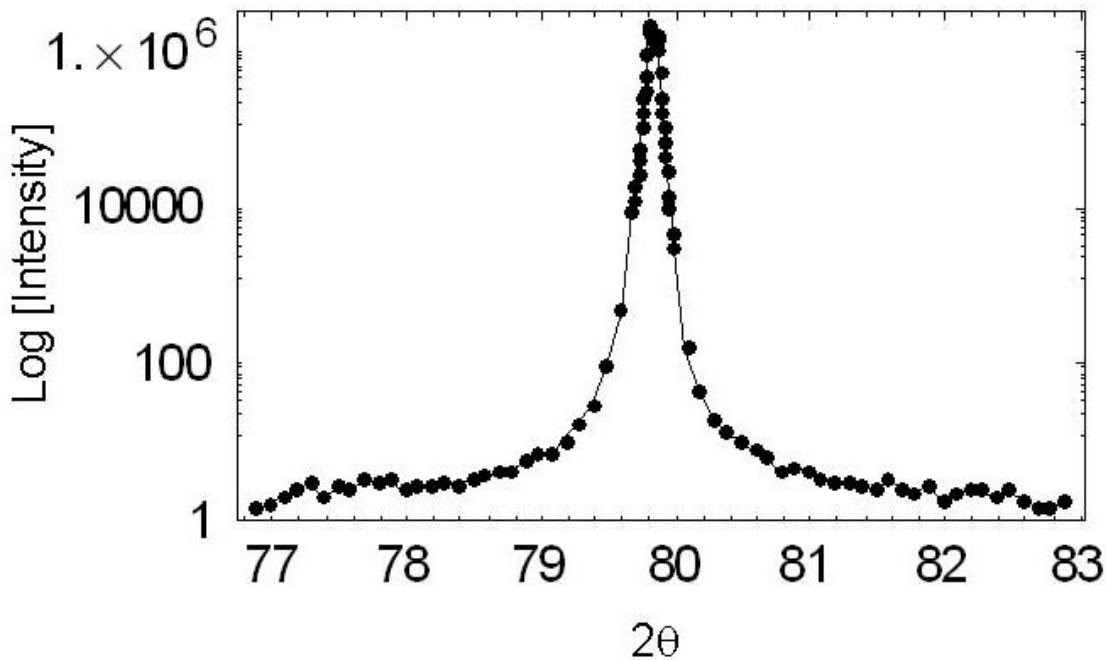

Figure 4. Radial scan of intensity through (080) fundamental reflection.

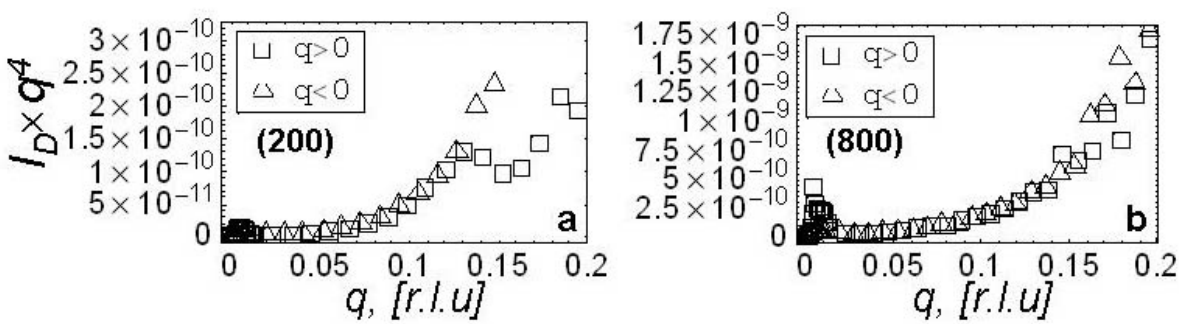

Figure 5. The diffuse intensity for positive (open squares) and negative (open triangles) *q* values along the radial direction: (a) (200); (b) (080) reflections.

Bragg peak positions. The intensity profile along the diffraction vector of the fundamental (800) reflection is shown in Fig. 4. The intensity profile is only slightly asymmetric.

To emphasize the *q* dependence of the intensity, the diffuse intensity is scaled by q^4. The product $I_D(q) \times q^4$ is shown in Fig.4 for different *q* values in reciprocal space for (020) and (080) reflections. We observe that the intensity distributions for positive and negative *q* are symmetric except for the narrow central region occupied by the regular Bragg component (this is in contrast to the case of diffuse scattering behavior due to vacancy or interstitial clusters observed in [4-6]). At higher *q* values oscillations of the diffuse

scattering intensity are observed. These oscillations are in line with the theoretical model proposed by Trinkaus [8]. It is possible to show that such oscillations should be most distinct for reflections with smaller *H* and are washed out at higher *H* values as is observed in our results (compare open squares for (200) and (800) reflections in Fig. 4). The size and shape of the precipitates determined from the analysis of the superstructure reflections were used as a input parameters for simulations of diffuse scattering contourmaps around fundamental reflections. Experimental and simulated maps of the intensity around the (800) reflection are shown in the Fig. 6. Simulations were performed for the model of strain fields caused by coherent precipitates in the disordered Ni-based matrix without correlation between different precipitates.

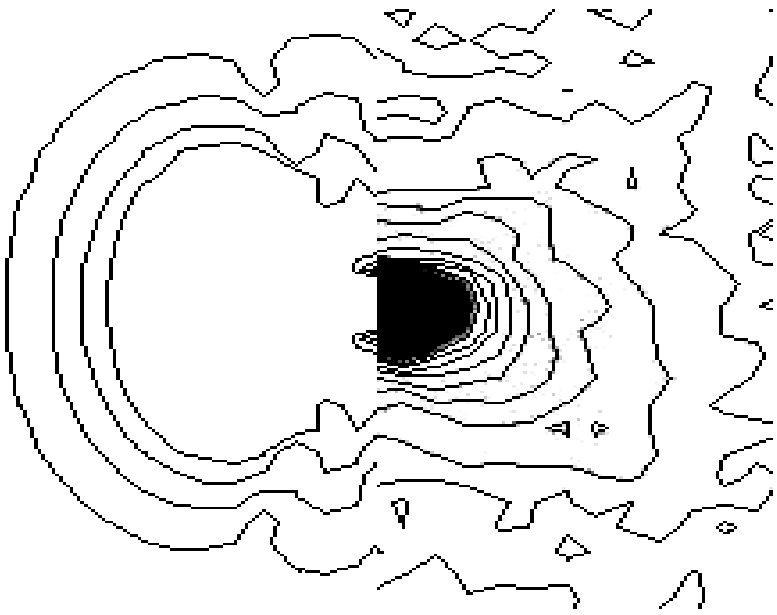

Fig.6 Simulated (left) and experimental (right) diffuse scattering map around the fundamental (800) reflection.

Summary

Diffuse scattering around both fundamental and superstructure reflections was considered for solids with coherent ordered precipitated. Shape function of the coherent precipitates was discussed. Diffuse scattering reveals precipitation induced strain in the matrix. The shape of the coherent precipitates is almost isotropic with an ~ 15% elongation along the stress annealing direction.

Acknowledgement

Research sponsored by the Division of Materials Sciences and Engineering, Office of Basic Energy Sciences and the ORNL SHARE user facility, U.S. Department of Energy, under Contract DE-AC05-00OR22725 with UT-Battelle, LLC. Work in part on Unicat

beamline 33-BM at the Advanced Photon Source (APS), which is supported by the University of Illinois at Urbana-Champaign, Materials Research Laboratory (U.S. DOE, the State of Illinois-IBHE-HECA, and the NSF), and by the Oak Ridge National Laboratory (U.S. DOE under contract with UT-Battelle LLC). The APS is supported by the U.S. DOE, Basic Energy Sciences, Office of Science under contract No. W-31-109-ENG-38.

References

1. M.A. Krivoglaz, *X-ray and Neutron Diffraction in Nonideal Crystals* (Berlin: Springer, 1996) p.465; *Theory of X-ray and Thermal Neutron Scattering by Real Crystals* (New York: Plenum, 1969) p.405.

2. R.I. Barabash, M.A. Krivoglaz, *Phys. Met. Metallogr*. **45** (1) (1978), 7-18; *Phys. Met. Metallogr*. **51** (5) (1981), 903-916.

3. R.I. Barabash, J.S. Chung, M.F. Thorpe, *J. Phys.: Condens. Matter* **11** (1999), 3075-3090.

4. S. Iida, B.C. Larson, J.Z. Tischler, *J. Mater. Res.* **3** (2) (1988), 267-273.

5. B.C. Larson, *J. Appl. Cryst.* **8** (2) (1975), 150-160.

6. B.C. Larson and W. Schmatz, *Phys. Rev.* B **10** 6 2307-2314 (1974).

7. P.H. Dederichs, *Phys.Rev.* B **4 (**4) (1971), 1041-1050.

8. H. Trinkaus, *Phys. Stat. Sol.* (b) **51**, (1972), 307-319.

9. C.R. Houska, *Acta Cryst.* A **49** (1993), 771-781.

10. O. Lyon, I. Guillon, C. Servant, *J. Appl. Cryst.* **34**, (2001), 484-492.

11. C. Servant, I. Guillon, O. Lyon, *J. Appl. Cryst.* **36**, (2003), 454-458.

12. A.G. Khachaturyan, *Theory of structural transformations in solids* (New York: Wiley & Sons, 1983) p.574

13. C. Wolverton, *Acta Mater*. **49** (2001), 3129-3142.

14. C. Wolverton, A. Zunger, *Phys.Rev.* B **49** (22) (1994), 16058 – 16061; **52** (1995), 8813-8828.

15. J. Wang, C. Wolverton, S. Muller, Z-K. Liu, L-Q. Chen, *Acta Mater*, (2005)

16. N.A. Zarkevich, D.D. Johnson, A.V. Smirnov, *Acta Mater.* **50** (2002) 2443-2459.

17. L-M. Stadler, B. Sepiol, R. Weinkamer, M. Hartmann, P. Fratzl, J.W. Kantelhardt, F. Zontone, G. Grubel, G. Vogl, *Phys. Rev.* B **68** (2003), 180101.

18. J.M. Schneider, B. Schonfeld, B. Deme and G. Kostorz, *J. Appl. Cryst*. **33** (2000), 465-468.

19. R. Drautz, H. Reihert, M. Fahnle, and H. Dosch, *PRL*, **87** (23) (2001), 236102.

20. L. Reinhard, J.L. Robertson, S.C. Moss, G.E. Ice, P. Zschack, C.J.Sparks, *Phys. Rev.* B **45** (6) (1992), 2662-2676.